Biochimica et Biophysica Acta 1837 (2014) 1235–1246

Contents lists available at ScienceDirect

Biochimica et Biophysica Acta

journal homepage: www.elsevier.com/locate/bbabio

Photoprotective sites in the violaxanthin–chlorophyll *a* binding Protein (VCP) from *Nannochloropsis gaditana*

Donatella Carbonera [a,*], Alessandro Agostini [a], Marilena Di Valentin [a], Caterina Gerotto [b], Stefania Basso [b], Giorgio Mario Giacometti [b], Tomas Morosinotto [b]

[a] Department of Chemical Sciences, University of Padova, Via Marzolo 1, 35131 Padova, Italy
[b] Department of Biology, University of Padova, via U. Bassi 58/B, 35121 Padova, Italy

ARTICLE INFO

Article history:
Received 31 January 2014
Received in revised form 18 March 2014
Accepted 25 March 2014
Available online 1 April 2014

Keywords:
Triplet state
VCP
Carotenoid
EPR
ODMR
Violaxanthin
Triplet–triplet energy transfer

ABSTRACT

Violaxanthin–chlorophyll *a* binding protein (VCP) is the major light harvesting complex (LHC) of the Heterokonta *Nannochloropsis gaditana*. It binds chlorophyll *a*, violaxanthin and vaucheriaxanthin, the last in the form of 19′ deca/octanoate esters. Photosynthetic apparatus of algae belonging to this group have been poorly characterized in the past, but they are now receiving an increasing interest also because of their possible biotechnological application in biofuel production. In this work, isolated VCP proteins have been studied by means of advanced EPR techniques in order to prove the presence of the photoprotective mechanism based on the triplet–triplet energy transfer (TTET), occurring between chlorophyll and carotenoid molecules. This process has been observed before in several light harvesting complexes belonging to various photosynthetic organisms. We used Optically Detected Magnetic Resonance (ODMR) to identify the triplet states populated by photoexcitation, and describe the optical properties of the chromophores carrying the triplet states. In parallel, time-resolved EPR (TR-EPR) and pulse EPR have been employed to get insight into the TTET mechanism and reveal the structural features of the pigment sites involved in photoprotection. The analysis of the spectroscopic data shows a strong similarity among VCP, FCP from diatoms and LHC-II from higher plants. Although these antenna proteins have differentiated sequences and bind different pigments, results suggest that in all members of the LHC superfamily there is a protein core with a conserved structural organization, represented by two central carotenoids surrounded by five chlorophyll *a* molecules, which plays a fundamental photoprotective role in Chl triplet quenching through carotenoid triplet formation.

1. Introduction

Photosynthetic organisms harvest sunlight thanks to the chlorophyll (Chl) and carotenoid (Car) molecules bound to the protein supercomplexes, embedded in the thylakoid membranes, called Photosystems I and II. Each photosystem is composed of two moieties, (i) the core complex, responsible for charge separation and first steps of electron transport, and (ii) the peripheral antenna system, with a role in light harvesting, transfer of excitation energy to the reaction centers, and photoprotective reactions, like quenching of Chl triplet and singlet excited states, and Reactive Oxygen Species (ROS) scavenging. Reaction centers are widely conserved among all organisms performing oxygenic photosynthesis, going from cyanobacteria to higher plants [1]. Antenna systems are instead far more diversified. In all eukaryotes, the antenna system is composed of members of a multigenic family of proteins called light harvesting complexes (LHC) proteins. All proteins belonging to this family have a common evolutionary origin [2–4] and share a conserved structural organization characterized by three membrane-spanning α-helixes connected by stroma and lumen-exposed loops. Two of these helixes are homologous and present a "generic LHC motif" consisting of a highly hydrophobic sequence containing glutamic acids involved in the Chl binding and in the stabilization of the folding through salt bridges with arginines in the other helix [5].

Despite this common origin, LHC proteins diversified in different groups of photosynthetic eukaryotes, such as Chl *a*/*b* binding proteins found in *Viridiplantae* (LHCA/LHCB), fucoxanthin Chl *a*/*c* binding protein (FCP, or LHCF) in diatoms, LHCR, in red algae and diatoms, and LHCSR/LHCX, with a role in photo-protection and found in all the above-mentioned groups [2,4,6,7]. Pigment binding properties of LHCs are thus diversified due to adaptation to the light availability in the specific habitat. Different LHCs can bind not only different Chl and Car species

Abbreviations: VCP, violaxanthin–chlorophyll *a* binding protein; Car, carotenoid; Chl, chlorophyll; LHC, light harvesting complex; FCP, fucoxanthin chlorophyll *a*/*c* binding protein; LHC-II, light harvesting complex of Photosystem II; ZFS, zero-field splitting; TR-EPR, Time-Resolved Electron Paramagnetic Resonance; TTET, triplet–triplet energy transfer; ODMR, optically detected magnetic resonance; FDMR, fluorescence detected magnetic resonance; T − S, triplet-minus-singlet

* Corresponding author. Tel.: +39 498275144; fax: +39 498275161.
E-mail address: donatella.carbonera@unipd.it (D. Carbonera).

http://dx.doi.org/10.1016/j.bbabio.2014.03.014
0005-2728/

but also pigments in different relative amounts, with the Chl/Car ratio that can change between the value of 3.5, observed in plants and green algae, and 0.9, characteristic of the fucoxanthin-chlorophyll proteins of diatoms [8].

Nannochloropsis gaditana is a eukaryotic alga belonging to *Eustigmatophyceae*, a group of organisms wich originated from a secondary endosymbiosis between an ancestor of red algae and a eukaryotic host cell [9]. The cells contain a single, big, chloroplast, which is surrounded by four membranes and occupies most of the cell volume. The *N. gaditana* photosynthetic apparatus is not well characterized although interest in this organism is increasing owing to its high rate of lipid productivity, which suggests that it could be a valuable candidate for biofuel production [10–12].

Photosystem II light harvesting proteins of *N. gaditana* are characterized by a particular pigment composition, different from the one of diatoms and any other known alga. In fact, they bind only Chl *a*, lack accessory Chls *b* or *c*, and have violaxanthin as the main accessory light harvesting pigment. Vaucheriaxanthin is present in minor amount, in the form of 19′ deca/octanoate esters [13–15]. For this reason, these antenna complexes have been defined violaxanthin–chlorophyll *a* binding proteins (VCP). The VCP fractions, purified from thylakoids solubilized in glycosidic detergents, have as a major component a 22-kDa polypeptide which, according to sequence analysis, shows similarity with LHCF from diatoms [16,17].

The number of chromophores bound *per* apoprotein is still unknown, however the ratio Chl/Car has been determined to be 1.7–1.8 and the ratio violaxanthin/vaucheriaxanthin is 1.5–1.6, depending on the oligomeric state of VCP [17].

It is well known that in light-stress conditions the formation of Chl triplet states (^{3}Chl) and singlet oxygen ($^1O_2$) in the photosynthetic apparatus may be particularly severe. In this scenario the constitutive mechanism of triplet–triplet energy transfer (TTET), played by carotenoids to quench ^{3}Chl *via* their triplet states, ($Car + {}^3Chl \rightarrow {}^3Car + Chl$), represents the fastest way of response before further photoprotective mechanisms have the time to take place. Once populated, ^{3}Car, lying at a lower energy compared to $^1O_2$, relaxes harmlessly to the ground state in the microsecond time scale [18]. TTET has been shown to occur in all the antennas of the LHC superfamily studied until now, in particular in FCP from *Cyclotella meneghiniana* [19,20], LHC from *Amphidinium carterae* [21] and LHC-II from *Spinacia oleracea* [22].

In this work, isolated VCP proteins from *N. gaditana* in different oligomeric states have been studied by means of advanced EPR techniques in order to investigate the presence of the photoprotective mechanism based on TTET. Optically Detected Magnetic Resonance (ODMR), time-resolved EPR (TR-EPR) and pulse EPR have been successfully employed in the past to get insights into the TTET mechanism in several light harvesting complexes [19–24]. The comparison of results obtained for VCPs with those previously published for other light harvesting complexes belonging to the LHC superfamily pointed out that, despite the divergence in sequence and pigment binding properties, they share a protein core, composed of five Chl *a* and two Car molecules, highly conserved also in the structural organization. This core has a major role in ^{3}Chl quenching and its photoprotective function is likely fundamental in all antenna systems of the LHC superfamily, as its conservation suggests.

2. Materials and methods

2.1. Cell growth

N. gaditana from CCAP, strain 849/5, was grown in sterile filtered F/2 medium [25], using sea salts 32 g/l from Sigma Aldrich, 40 mM TRIS/HCl pH 8, Sigma Aldrich Guillard's (F/2) marine water enrichment solution 1×. Cells were grown under 100 μE m^{-2} s^{-1} of illumination and mixed with air enriched with 5% CO_2. Temperature was set at 22 ± 1 °C.

2.2. VCP purification

Isolation of thylakoid membranes from *N. gaditana* was performed according to [17]. Thylakoid membranes were then solubilized with final 0.4% α-DM, 10 mM HEPES pH 7.5 and loaded in a 0.1–1 M sucrose gradient. The bands corresponding to monomeric and trimeric VCP of the sucrose gradient were then harvested with a syringe. All the manipulations performed to obtain final sampling for the ODMR and EPR experiments have been done in dim green light at 4 °C.

2.3. Sequence analysis

Alignment analysis was performed using T-Coffee [26,27] and manually modified with Bioedit 7.1.3.0. Chl binding sites were identified according to Liu et al. [5], α-helixes were named according to Dittami et al. [7]. *Nannochloropsis* sequences Naga 2 (Naga_100027g19), Naga3 (Naga_100012g50) Naga4 (Naga_100004g86) Naga9 (Naga_100017g59) and Naga17 (Naga_100013g28) were retrieved from nannochloropsis.org [28], while sequences from *Spinacia oleracea*, Lhcb1_So, (P12333.1), and *C. meneghiniana*, Fcp1_Cmen (AJ000670.1), were retrieved from NCBI.

2.4. ODMR measurements

The principle of the ODMR technique, reviewed in [29], will be briefly summarized in the following. ODMR is a double resonance technique based on the principle that, when a triplet steady state population is generated under continuous illumination, the application of a resonant microwave electromagnetic field between a couple of spin sublevels of the triplet state, generally induces a change of the steady state population of the triplet state itself, due to the anisotropy of the decay and population rates of the spin sublevels. The induced change of the triplet population may be detected as a corresponding change of the emission and/or absorption of the system. In particular, absorbance detected magnetic resonance (ADMR), detects the change in the steady state absorption of the chromophore carrying the triplet state, whereas the changes in the emission are detected by means of fluorescence detected magnetic resonance (FDMR).

FDMR and ADMR experiments were performed in the laboratory built apparatus, described in detail in [30,31]. Amplitude modulation of the applied microwave field is used to greatly increase the signal to

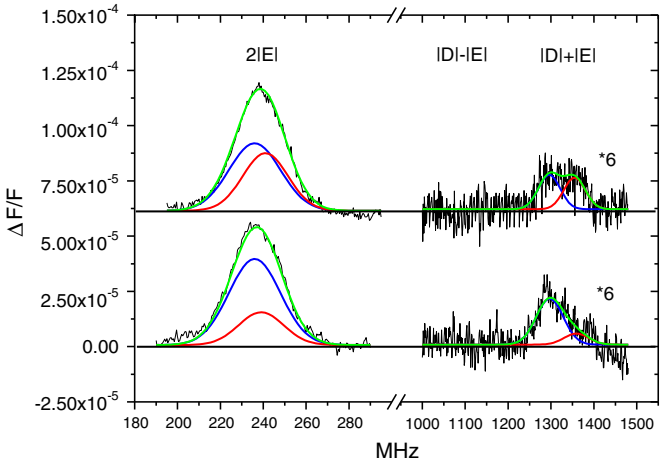

Fig. 1. ^{3}Car FDMR spectra of monomeric (top) and trimeric (bottom) VCPs detected at 690 nm. Amplitude modulation frequency: 333 Hz, time constant: 600 ms, temperature: 1.8 K. Reconstruction (green) of the experimental spectra (black) using two Gaussian components (blue and red). Spectra vertically shifted for comparison.

noise ratio by means of a phase sensitive lock-in amplifier (EG&G 5220). In the FDMR experiments the fluorescence, excited by a halogen lamp (250 W) focused on the sample and filtered by a broadband 5 cm solution of $CuSO_4$ 1 M, was collected at 45° through appropriate band-pass filters (10 nm FWHM) by a photodiode. The photodiode signal was demodulated after entering the lock-in amplifier.

Low temperature emission spectra were detected in the same apparatus used for ODMR experiments, using the same excitation source, but substituting the band-pass filters, before the detector, by a monochromator. In ADMR, the same excitation lamp was used but without filters before the sample, except for 5 cm water and heat filters. The beam was focused on the monochromator after passing the sample and finally collected by the photodiode. The amplitude modulation frequency and the microwave power were chosen depending on the experiment.

By fixing the microwave frequency at a resonant value and sweeping the detection wavelength, microwave-induced Triplet-minus-Singlet (T−S) spectra were registered.

Compared to time-resolved absorbance spectroscopy on the triplet state, the ODMR technique allows selection (by the microwave field) of different triplet components which can be, in this way, well distinguished to each other and optically characterized.

The temperature of all the experiments performed on VCP was 1.8 K. At this temperature spin-lattice relaxation is inhibited and the ODMR signal is detectable.

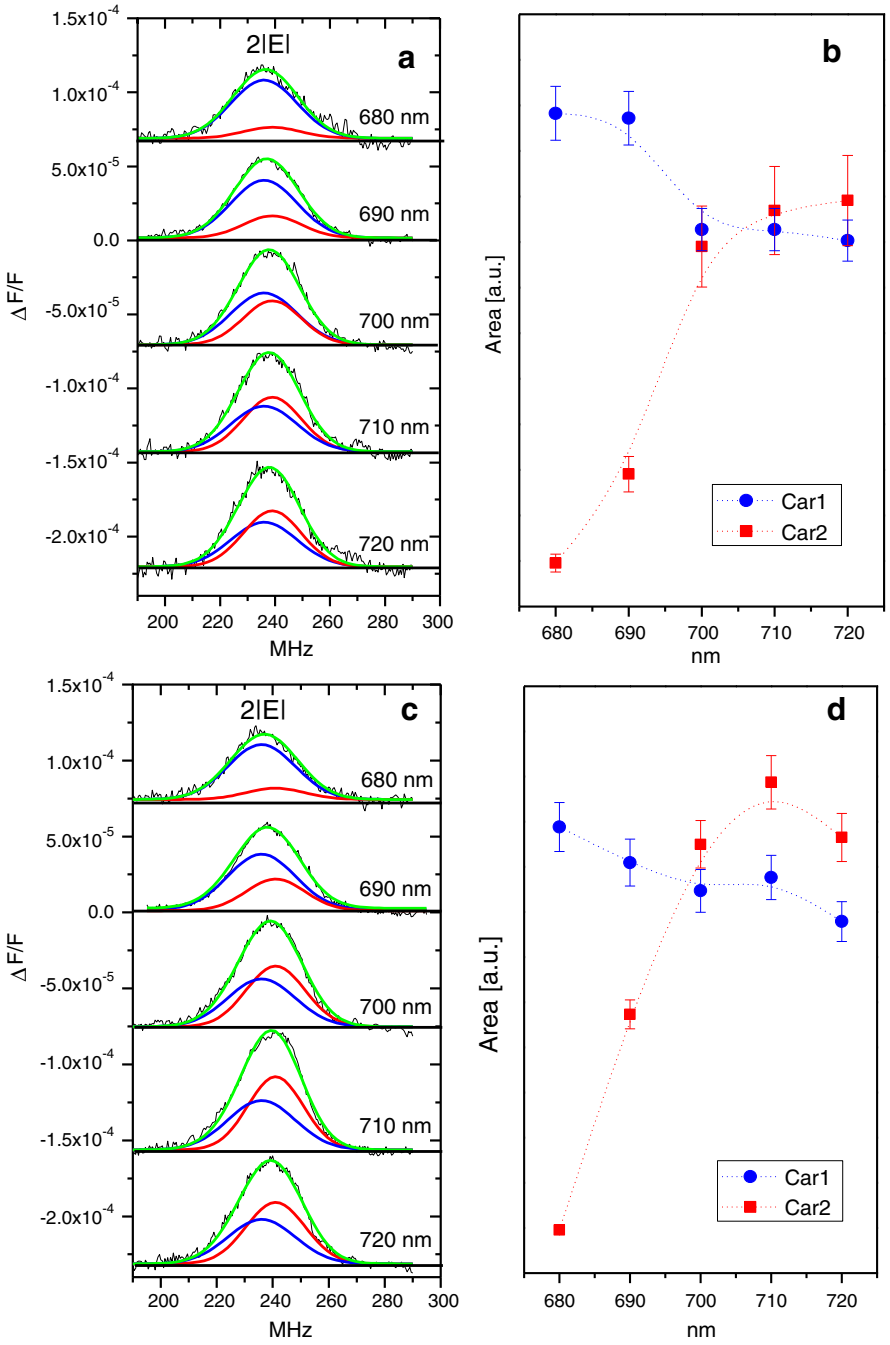

Fig. 2. 2|E| FDMR transitions (black, left panels) of ^{3}Car detected at different wavelengths in the 680–720 nm range, as indicated. (a) Monomer, (c) trimer VCP. Experimental condition as reported in the caption of Fig. 1. Spectra vertically shifted for better comparison. Left panels (a,c): reconstruction (green) of the experimental spectra using two Gaussian components (blue and red). Right panels: amplitude dependence (area of the corresponding Gaussian curves) of the two triplet components on the detection wavelength: (b) monomer, (d) and trimer.

The samples were diluted to a final Chl concentration of 100 μg/ml. Immediately before the insertion into the cryostat, degassed glycerol was added to the samples to a final concentration of 60% v/v, in order to obtain homogeneous and transparent matrices upon freezing.

2.5. TR-EPR and pulse EPR measurements

TR-EPR experiments were performed using a modified Bruker ER200D spectrometer with an extended detection bandwidth (6 MHz), disabling magnetic field modulation and using pulsed photo-excitation from the second harmonic of a Nd:YAG pulsed laser (Quantel Brilliant, λ = 532 nm pulse length = 5 ns, pulse energy = 5 mJ, repetition rate = 20 Hz). The spectrometer was equipped with a nitrogen flow cryostat for sample temperature control (110–400 K). The signal was recorded with a LeCroy LT344 digital oscilloscope, triggered by the laser pulse. Transient signal rise time was about 150 ns. The experiments were carried out with a microwave power in the cavity of 2 mW.

Pulse EPR experiments were performed on an X-band Bruker Elexsys E580 pulsed EPR spectrometer equipped with an optically transparent dielectric ring EPR/ENDOR resonator (ER4118X-MD5W1). The temperature was controlled by means of a liquid helium flow cryostat with optical access (Oxford CF935O) driven by a temperature controller (Oxford ITC503). Pulsed laser excitation was provided by the second harmonic (532 nm) of a Quantel Brilliant Nd:YAG laser (5 mJ per pulse and repetition rate of 10 Hz). Field-swept electron spin echo (FSE) spectra were recorded using a 2-ESE sequence pulse (flash-DAF-π/2-τ-π-τ-echo).

The samples were diluted to a final Chl concentration of 100 μg/ml. Glycerol was added to the samples to a final concentration of 60% v/v.

2.6. Triplet–triplet energy transfer and spectral simulations

If the TTET mechanism is operating, the Car inherits the polarization of the Chl in a way which depends on the relative geometrical arrangement of the donor–acceptor couple. Calculations of the triplet state sublevel populations of the acceptor, starting from those of the donor, in the hypothesis of spin momentum conservation during TTET, were performed as before for LHC-II, LHC, FCP and PCP complexes [20–24] (a brief description is reported in the Supplementary material), using a home-written program in MatLab® software, following the formalism of Brenner et al. [24,32]. The directions of the ZFS axes and the order of the energy sublevels of the carotenoid triplet state were taken as those of lutein triplet state in LHC-II [22]. Simulations of the powder spin-polarized triplet spectra were performed using a program written in MatLab®, with the aid of the Easyspin routine (ver. 2.6.0), [33] based on the full diagonalization of the triplet state spin Hamiltonian, including the Zeeman and magnetic dipole–dipole interactions, considering a powder distribution of molecular orientations with respect to the magnetic field direction. Input parameters are the triplet state sublevel populations, the zero-field splitting (ZFS) parameters, the linewidth at the canonical orientations, and the g-tensor components.

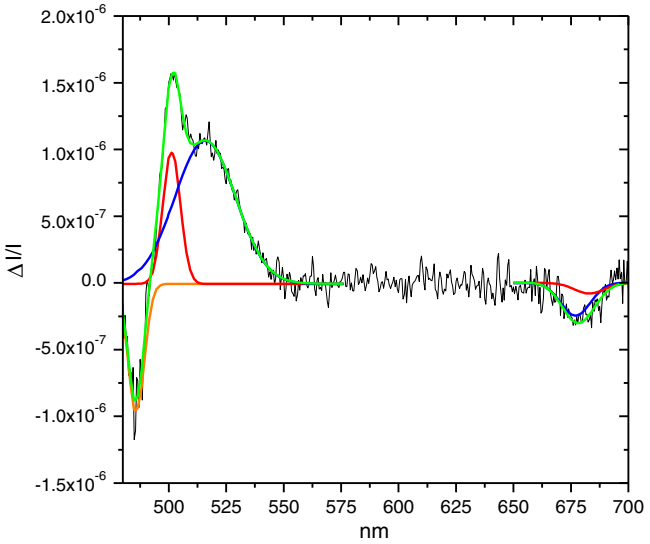

Fig. 3. T−S spectrum of trimeric VCP (black) detected at 237 MHz (2|E| transition of ^{3}Car). Amplitude modulation frequency, 333 Hz, time constant: 3 s, temperature 1.8 K, slit 1.0 nm, 6 scans. Reconstruction (green) of the T−S spectrum, using Gaussian components (orange, blue and red).

3. Results

3.1. ODMR of ^{3}Car

Illumination of the VCP at cryogenic temperatures leads to the formation of a steady state population of ^{3}Car which can be detected by FDMR, by monitoring the emission of the sample while sweeping the microwave field, as previously reported for other antenna complexes [19,21,30,34]. The spectra of monomeric and trimeric VCP samples, detected at 690 nm, are reported in Fig. 1. The assignment to ^{3}Car can be easily done on the basis of ZFS parameters (D and E) [30, 34,35]. The 2|E| transition of ^{3}Car is the most intense followed by the |D|+|E| transition. The |D|−|E| transition, expected between 1000 and 1100 MHz, was too weak to be discernible from the noise. Although carotenoids are non-fluorescing molecules, their FDMR transitions can be detected indirectly *via* the Chl emission, because of the energy transfer processes (both singlet–singlet and triplet–triplet) occurring among carotenoids and chlorophylls in the antenna complexes. In fact, a change of the steady state population of the ^{3}Car states, induced by a resonant microwave field, is reflected by a change of the intensity of the fluorescence of the nearby Chl molecules connected *via* energy transfer [30].

Since carotenoid triplet states are not populated directly from their excited singlet states, due to their intrinsic low probability of ISC, the occurrence of ^{3}Car signals in the FDMR spectra of VCP, observed by monitoring the Chl *a* fluorescence, is a strong evidence that the main light harvesting complex of *N. gaditana* is active in triplet–triplet energy transfer as a mechanism for ^{3}Chl deactivation.

Table 1
Parameters[a] for the reconstruction of ^{3}Car FDMR spectra shown in Figs. 1 and 2, using Gaussian components $\left(y = \frac{A_i}{w\sqrt{\pi/2}} e^{\frac{2(x-x_c)^2}{w^2}}\right)$ and characteristic absorption maxima[b] of the T−S spectrum shown in Fig. 3.

Triplet	2|E|		|D| + |E|		|D| [cm^{-1}]	|E| [cm^{-1}]	Triplet–triplet absorption λ [nm]	Q_y transition of interacting chlorophyll λ [nm]
	x_c [MHz]	FWHM [MHz]	x_c [MHz]	FWHM [MHz]				
Car1	236.0 ± 0.2	24 ± 1	1297.0 ± 0.5	30 ± 1	0.0393 ± 0.0001	0.00394 ± 0.00002	515.8 ± 0.7	668.0 ± 0.5
Car2	239.0 ± 0.2	21 ± 1	1360.0 ± 0.5	30 ± 1	0.0414 ± 0.0001	0.00399 ± 0.00002	501.3 ± 0.1	678.0 ± 0.2

[a] D| and |E|: ZFS parameters. x_c: center of the Gaussian, FWHM = full width at half maximum. Relative amplitude is shown in Fig. 2.
[b] In the last two columns the maximum of the T–T absorption and of the bleaching of the Q_y transitions assigned to interacting Chls, of the T−S spectra shown in Fig. 3, is reported.

The FDMR spectra of VCP have been measured by monitoring the Chl *a* emission at different wavelengths in the range between 680 and 720 nm. Although the |D|+|E| transition was very weak and allowed a reliable detection only at 690 nm, a complete trend of the 2|E| transition *vs* the detection wavelength is reported in Fig. 2, for both monomeric and trimeric VCPs. The spectra in the two different oligomeric states are nearly identical, suggesting the involvement of the same photoprotective sites. The asymmetry of the |D|+|E| and the observed wavelength dependence of the 2|E| transitions, indicates the presence of at least two different ^{3}Car species. In the global fitting of the FDMR data, the spectra were reconstructed considering only two components (Figs. 1, 2 and Table 1), namely Car1 (|D| 1179 ± 5 MHz, |E| 118 ± 2 MHz) and Car2 (|D| 1240 ± 5 MHz, |E| 120 ± 2 MHz).

The microwave induced T−S spectrum of ^{3}Car detected at 237 MHz, *i.e.* at the maximum of the 2|E| transition observed in the FDMR spectra, is shown in Fig. 3 for monomeric VCP. No substantial differences were observed in trimeric VCP (Fig. S1, Supplementary material). The composite triplet–triplet absorption of the microwave induced T−S spectrum detected at 237 MHz, in the region comprised between 480 and 570 nm has been fitted with two Gaussian components (Fig. 3, Table 1). The occurrence of two bands in the T−S spectrum detected at the maximum of ^{3}Car 2|E| transition was previously reported for LHC-II (for comparison, the spectrum of LHC-II is reported in Fig. S1, Supplementary material) [30,35,36]. The broad bleaching between 600 and 700 nm is generated from Chls. Analogous bands have been observed in the past in the ^{3}Car T−S spectra of several light harvesting complexes [21,35,37,38] and they correspond to a decrease of Chl *a* absorption when the ^{3}Car population is increased by the resonant microwave field. A decrease of the Car singlet absorption is also observed (at about 490 nm) as a consequence of the increase of the ^{3}Car population, which leads to a decrease of the Car ground state population. In a different way, the bleaching of the Chls bands is not due to a decrease

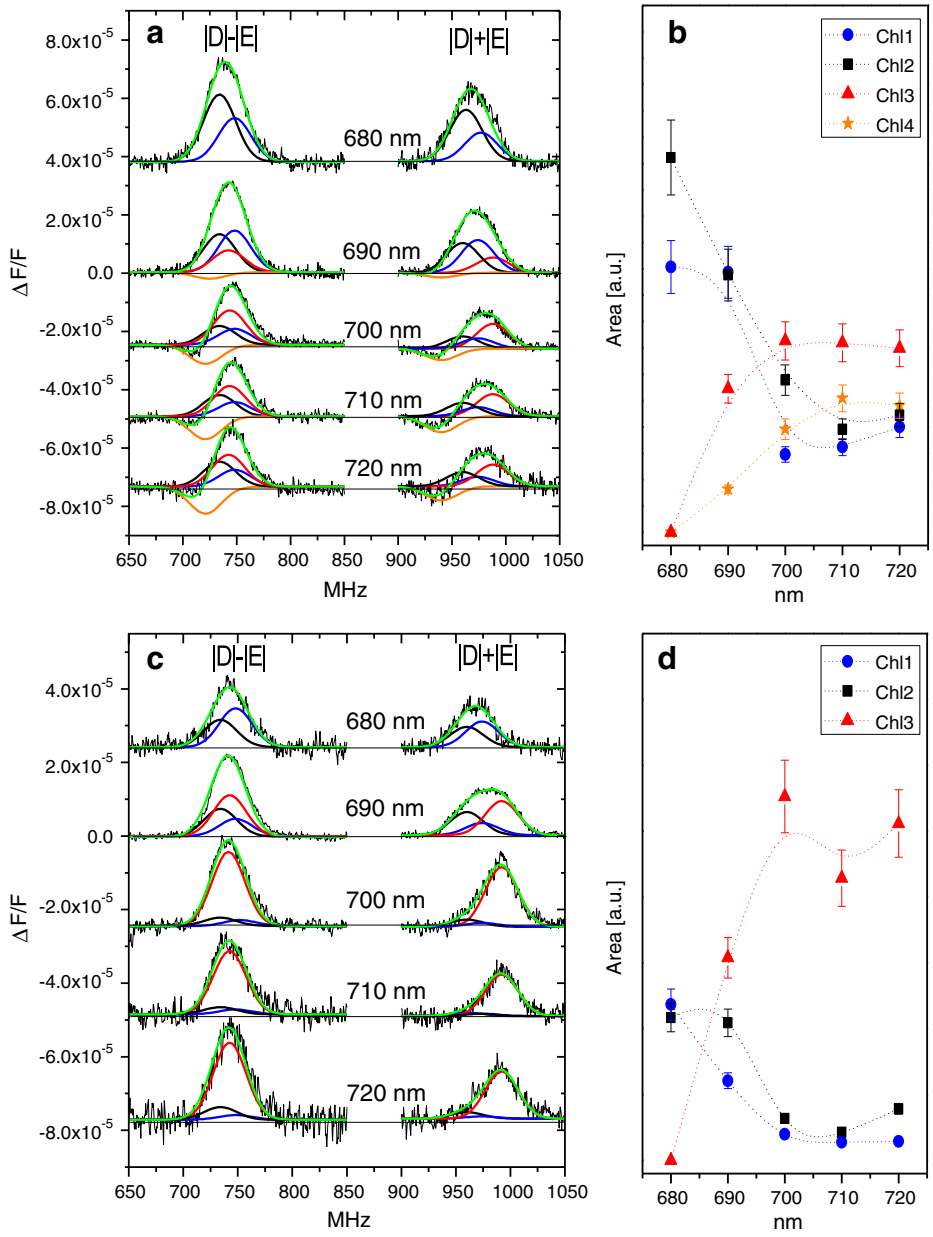

Fig. 4. |D|+|E| and |D|−|E| transitions of the FDMR spectra (black thin, left panels) of ^{3}Chl detected at different wavelengths in the 680–720 nm range, as indicated. (a) Monomer, (c) trimer VCP. Amplitude modulation 333 Hz, time constant 600 ms, temperature 1.8 K. Spectra vertically shifted for better comparison. Left panels: reconstruction (green) of the experimental spectra with Gaussian components (blue, black thick, red and orange). Right panels: amplitude dependence (averaged area of the corresponding Gaussian components fitting the |D|+|E| and |D|−|E| transitions) of the triplet components on the detection wavelength for monomers (b), and trimers (d) respectively.

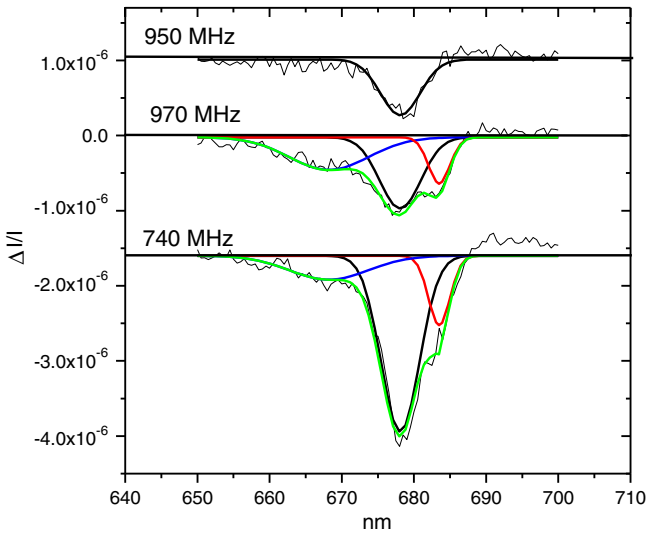

Fig. 5. T−S spectra of ^{3}Chl of trimeric VCP (black thin), measured at different frequencies as indicated. Amplitude modulation frequency, 33 Hz, time constant: 3 s, temperature 1.8 K, slit 1.0 nm, 6 scans. Spectra vertically shifted for better comparison. Reconstruction (green) of the experimental spectra using Gaussian components (blue, black thick and red). Color code as in Fig. 4.

of the Chl ground state population, rather, as suggested before for analogous spectral features [21,35,37,38], to a change of the electronic properties of the Chls interacting with the nearby Cars carrying the triplet state. When the electronic distribution of carotenoids changes, going from singlet to triplet, the interaction with the Chls is affected, leading to a change of the optical density (and/or a shift of the wavelength maximum) of their Q-bands. In VCP the broad bleaching between 600 and 700 nm has been reconstructed with two components (Fig. 3, Table 1) because, although the Chl Q-band bleaching is not well resolved into two components as in LHC-II, however the linewidth corresponds to two overlapping bands (at 1.8 K), suggesting the presence of at least two distinct Chls *a* interacting with the two different carotenoids carrying the triplet states. The two ^{3}Car components, assigned to different carotenoid triplet states, show different detection wavelength dependence, in the associated FDMR spectra. The more intense component, indicated as Car1, which corresponds to the Car with a triplet–triplet absorption centered at 516 nm, is detected from the fluorescence of a Chl *a* with a "bluer" emission (Fig. 2b, d), while the minor component (Car2), which has a triplet–triplet absorption centered at 501 nm, is detected preferentially at longer wavelengths in the FDMR spectra. Thus, as in the case of LHC-II (Fig. S1, Supplementary material) [30,35,36,39], the ^{3}Car red component is interacting with the bluer Chl, having the Q-band bleaching at 677 nm, and *vice versa* the ^{3}Car blue component, interacts with the Chl absorbing at 683 nm.

Furthermore, from the analysis of both the T−S and FDMR spectra, it can be pointed out that monomeric and trimeric VCPs share the same photoprotective couple of carotenoids (not shown).

3.2. ODMR of ^{3}Chl

In order to verify the presence of unquenched ^{3}Chl, corresponding to Chls disconnected to Cars, the FDMR spectra have been also collected with a ten times lower frequency of the amplitude modulation (*i.e.* 33 Hz), which is selective for the detection of slowly decaying triplet states as ^{3}Chl. The FDMR spectra have been measured collecting the emission in the range between 680 and 720 nm, in the microwave field region where the |D|−|E| and |D|+|E| transitions of ^{3}Chl *a* states are expected [30] (Fig. 4 a, c). Chls have an intensity pattern of the zero-field transitions inverted with respect to the one of carotenoids, with a 2|E| transition usually too weak to be detected, as found here in the VCP.

The presence of a steady state population of ^{3}Chl under illumination of the sample means that the ^{3}Chl deactivation *via* TTET by Car in VCP is not complete, at least in the isolated protein complex and at the low temperature of the experiments. The |D|−|E| and |D|+|E| transitions show a lineshape dependence on the detection wavelength, due to the presence of distinct ^{3}Chl pools, characterized by different optical and magnetic properties. This wavelength dependence of the transitions is more prominent for the trimeric VCP, while the monomer manifests a smoother variation. Moreover, the profiles of both bands in the monomer display small negative contributions around 710 MHz and 932 MHz in the FDMR spectra detected between 700 and 720 nm that are not present in the spectra of the trimer. This is an indication that at least one extra "red" pool of ^{3}Chl is present in monomeric VCP.

As in the case of ^{3}Car, in order to disentangle the different overlapping components contributing to the FDMR spectra, we recorded the T−S spectra and performed a global analysis.

The T−S spectra of VCP in the range 650–700 nm, measured at three different microwave frequencies, are reported in Fig. 5. No substantial differences have been revealed between the two forms of VCP. The T−S spectra have been fitted by means of three Gaussian components, corresponding to three different pools of unquenched ^{3}Chl centered at 667, 677, 685 nm (bleaching positions in the T−S spectra), showing that red forms are present in VCP and that triplet states can be populated also in "blue" Chls. The minimum number of triplet components obtained from the analysis of the T−S spectra has also been used in the global fitting procedure of the FDMR spectra, as reported in Fig. 4 (a, b, c, d) and Table 2. The FDMR spectra of both forms of VCP share these three components. However, in order to obtain a good fit in the case of monomeric VCP an additional minor component (Chl4) was added, (Fig. 4 c). Due to the low intensity of this component an associated T−S spectrum was not detected.

3.3. TR-EPR and pulse EPR

Since time-resolved and pulse EPR may give important information on the relative geometry of the pigments involved in the triplet–triplet energy transfer occurring in VCP, we performed also these kinds of experiments to better characterize the photoprotective sites.

The 125 K X-band TR-EPR spectra of monomeric VCP, detected at different delay times after the laser flash, show the presence of an intense

Table 2
Parameters[a] for the reconstruction of ^{3}Chl FDMR spectra, shown in Fig. 4, using Gaussian components $\left(y = \frac{A_i}{w\sqrt{\pi/2}} e^{\frac{2(x-x_c)^2}{w^2}}\right)$, and characteristic absorption maxima[b] of the T−S spectra shown in Fig. 5.

Triplet	|D| − |E|		|D| + |E|		|D| [cm^{-1}]	|E| [cm^{-1}]	Singlet–singlet absorption λ [nm]
	x_c [MHz]	FWHM [MHz]	x_c [MHz]	FWHM [MHz]			
Chl1	748.0 ± 0.5	30 ± 1	974.0 ± 0.5	30 ± 1	0.0288 ± 0.0001	0.00378 ± 0.00002	668.0 ± 0.5
Chl2	734.0 ± 0.5	30 ± 1	960.0 ± 0.5	30 ± 1	0.0283 ± 0.0001	0.00378 ± 0.00002	678.0 ± 0.2
Chl3	742.5 ± 0.5	30 ± 1	992.0 ± 0.5	30 ± 1	0.0290 ± 0.0001	0.00417 ± 0.00002	684.0 ± 0.2
Chl4	742.5 ± 0.5	30 ± 1	940.0 ± 0.5	30 ± 1	0.0278 ± 0.0001	0.00366 ± 0.00002	n. d.

[a] |D| and |E|: ZFS parameters. x_c: center of the Gaussian, FWHM = full width at half maximum. Relative amplitudes are shown in Fig. 4.
[b] In the last column the maximum of the Q_y band bleaching of the associated T−S spectrum is reported.

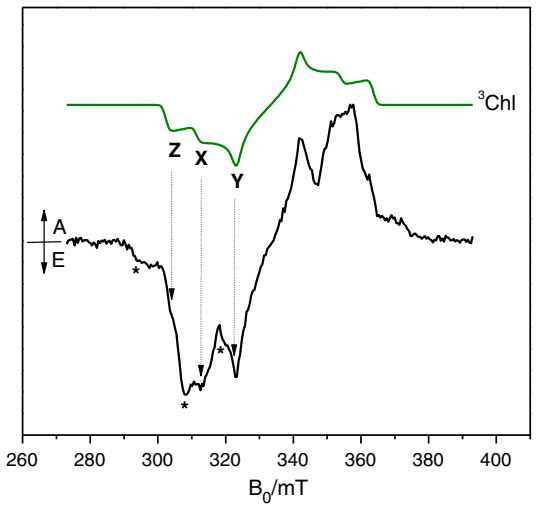

Fig. 6. TR-EPR spectrum of VCP (black), taken 150 ns after the laser pulse at 125 K, and ^{3}Chl spectrum (green) calculated according to the parameters reported in Table 3 for ^{3}Chl. X, Y and Z represent the ZFS canonical orientations. The features which arise from the ^{3}Car contribution are marked with asterisks (*).

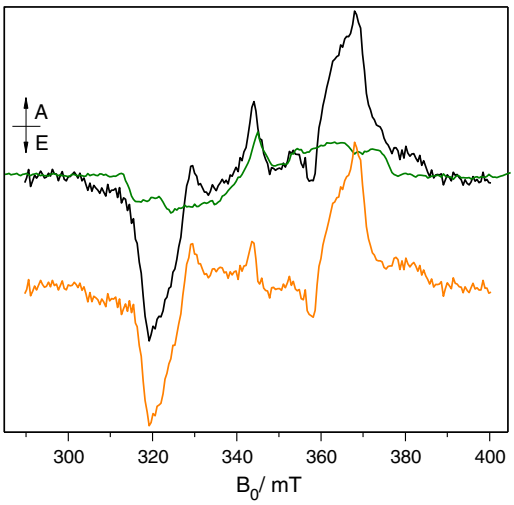

Fig. 7. FSE spectrum of VCP (black), and ^{3}Chl dissolved in micelles of Triton X-100 (green) [22], taken immediately after the laser flash at 20 K. The bottom trace represents the difference between the FSE spectrum of VCP and the FSE spectrum of ^{3} Chl and corresponds to the "pure" ^{3}Car spectrum (orange curve).

photo-generated spin-polarized signal (Fig. 6). The spectrum detected immediately after the laser flash, reveals the presence of ^{3}Car and ^{3}Chl *a*. In fact, the different ZFS parameters allow us to assign the pair of strong signals (at 323 and 342.5 mT) to the low and high field Y ZFS transitions of the ^{3}Chl. In the regions between 301–318 and 347–364 mT, the triplet spectra of the two chromophores largely overlap, but at fields lower than 301 and higher than 364 mT only the Z transitions of ^{3}Car contribute. The time evolution of the TR-EPR spectrum follows the common behavior reported for ^{3}Chl and ^{3}Car triplet states [40–42] (data not shown). The ^{3}Chl signal is due to those Chls in the protein which are not able to transfer the triplet excitation to carotenoids and therefore represent an "unquenched" ^{3}Chl population. "Unquenched" ^{3}Chls have been detected in previous TR-EPR studies on other light harvesting proteins homologous to VCP, such as LHC-II from higher plants, [22] LHC from dinoflagellates [21] and FCP from diatoms. [20]. In those complexes, the ^{3}Chl polarization pattern was *eeeaaa*, the same observed also for ^{3}Chl *a* dissolved in micelles of Triton X100 [22]. The corresponding sublevel population rates, used in the reconstruction of TR-EPR spectra [21,22], have been used also in the present analysis as input parameters for the calculation of the spectral contribution of ^{3}Chl to the TR-EPR spectrum of VCP (together with the ZFS parameters |E| = 40 G and |D| = 307 G, representing average values of those derived from the ODMR results) (Fig. 6, Table 3).

Two-pulse ESE experiments have been successfully used before for the analysis of the EPR spectra of the photo-induced triplet states in LHC-II [22]. We have previously demonstrated that for ^{3}Car states, the shape of TR-EPR and FSE spectra, taken at short delay after the laser flash (DAF), are identical [23]. In contrast, ^{3}Chl are known to show anisotropic relaxation processes which are reflected in their FSE spectra [23]. This characteristic can be exploited to determine experimentally the polarization pattern of ^{3}Car, which is essential to get a reliable estimate of the geometry of the Chl–Car couples involved in TTET. In Fig. 7 we report the FSE spectrum of VCP and of ^{3}Chl dissolved in Triton X-100 1 mM, detected at the same τ and DAF as for VCP. It can be seen that the shape of the FSE spectrum of ^{3}Chl is different from the corresponding TR-EPR, shown in Fig. 6. A comparison of the FSE and TR-EPR spectra of VCP (reported in Figs. 7 and 6 respectively), reveals that, as expected, the spectral contribution of ^{3}Chl is strongly reduced in the FSE spectrum, especially in correspondence to the central lines attributed to the Y canonical ZFS orientation of the ^{3}Chl. This spectral effect makes the FSE spectrum a good starting point for determining the "pure" contribution of ^{3}Car. In fact, by subtracting an appropriate amount of the experimental ^{3}Chl *a* FSE spectrum from that of VCP, the pure contribution of ^{3}Car is obtained (orange curve in Fig. 7). The best subtraction has been obtained by minimizing the spectral features due to ^{3}Chl in the difference spectrum. Note that a contribution from a radical species is also present in the center of the spectrum. The pure contribution of ^{3}Car triplet state shows a polarization (*eeaeaa*) which is very similar to the one obtained for LHC-II [22] (in Fig. S3 in Supplementary material the comparison between the two light harvesting complexes is reported).

3.4. Model of pigment arrangement in VCP

Led by the observed similarity of the ODMR and EPR results on VCP with those previously obtained on LHC-II, we have determined the sequence homology between the two proteins to evaluate the possibility to use the available LHC-II structural data [5] (PDB ID: 1RWT) as a starting point for a model structure of VCP. The polypeptide composition of the samples investigated by ODMR and TR-EPR is not precisely known since, as for LHC-II in plants, it is composed by a mixture of similar proteins. However, its most abundant component has been

Table 3
Parameters[a] of triplet state simulations for the reconstruction of TR-EPR spectra reported in Fig. 11.

Triplet	|E| [mT]	|D| [mT]	P_x:P_y:P_z	W_x:W_y:W_z [mT]	Relative contribution
Chl *a* "unquenched"	4.0 ± 0.1	30.7 ± 0.1	0.375:0.425:0.200	2.5 ± 0.1:2.5 ± 0.1:2.5 ± 0.1	1
Car populated from Chl *a* 612	4.0 ± 0.1	41.0 ± 0.1	0.35:0.28:0.37	2.0 ± 0.1:2.0 ± 0.1:2.0 ± 0.1	0.7
Car populated from Chl *a* 610	4.0 ± 0.1	41.0 ± 0.1	0.41:0.21:0.38	2.0 ± 0.1:2.0 ± 0.1:2.0 ± 0.1	0.5

[a] $P_{x,y,z}$: zero-field populations ($P_{x,y,z}$) of Car are derived by calculation of TTET starting from Chl *a* 612 and Chl *a* 610 triplet states. Zero-field populations ($P_{x,y,z}$) of Chl *a* are used for both the TTET calculations and for "unquenched" ^{3}Chl *a* contribution to the experimental spectrum. |D| and |E|: ZFS parameters. Wi: line width at the canonical positions in the EPR powder spectrum.

identified and sequenced [16,43], while other LHC isoforms similar to this first VCP polypeptide can be identified in *N. gaditana* genome (Fig. 8). The alignment of the sequences from *N. gaditana* with Lhcb [5], the major component of LHC-II from *S. oleracea*, and Fcp1, [44] the gene of the main peptide present in FCP from the diatom *C. meneghiniana* [45], shows that most conserved regions in the amino acid sequences are the three transmembrane α-helixes (Fig. 8). In these helixes five amino acids involved in the binding of Chl *a* molecules

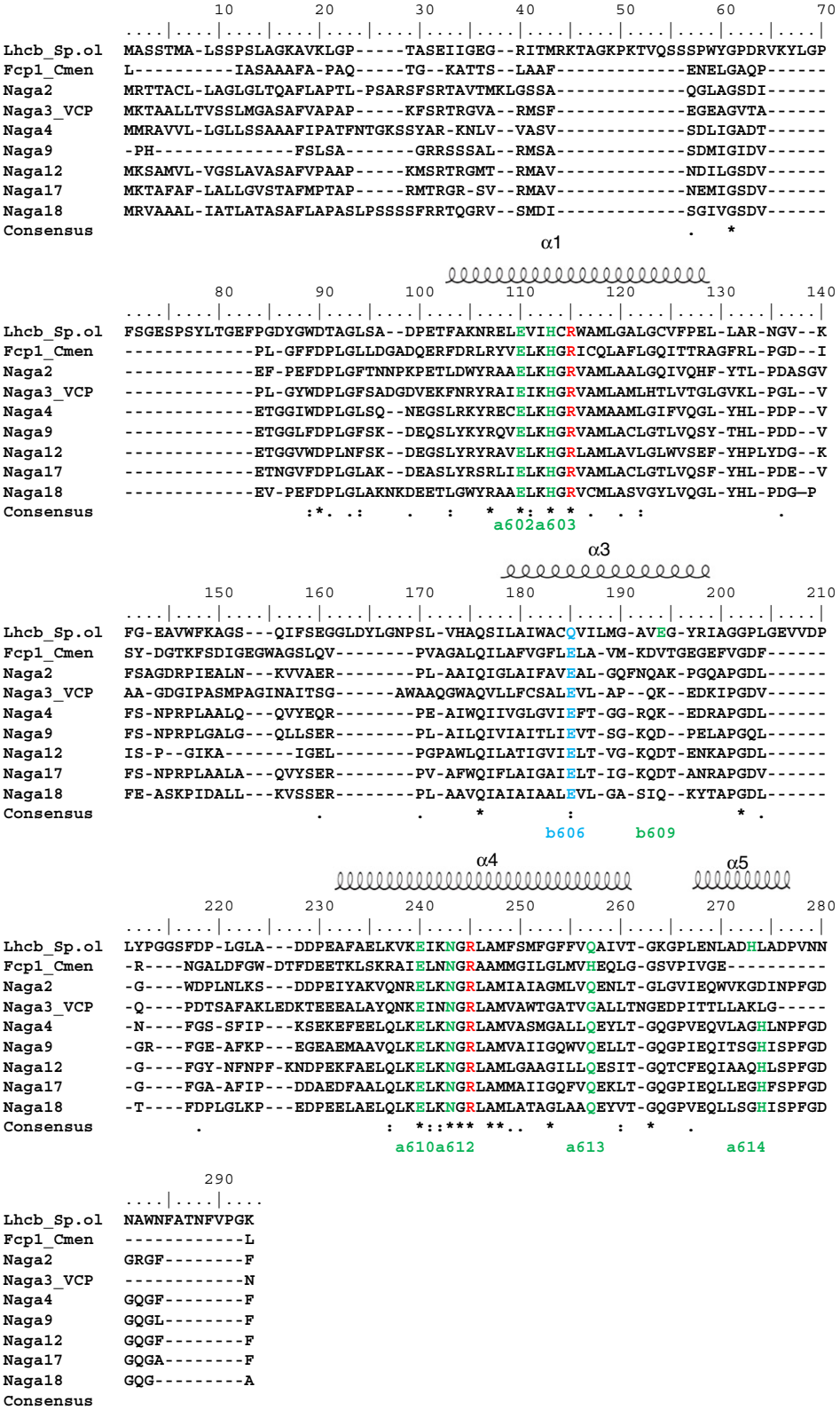

Fig. 8. Polypeptide sequence alignment of the VCP genes from *N. gaditana* (Naga) with Lhcb from *S. oleracea* and Fcp from *C. meneghiniana*; α-helices are named according to Dittami et al. [7]. Residues are color-coded: Chl *a* side chain ligand (green), Chl *b* side chain ligand (blue); Arg in salt bridge to Glu residue in the other helix (red). The program T-Coffee was used for the alignment [26,27].

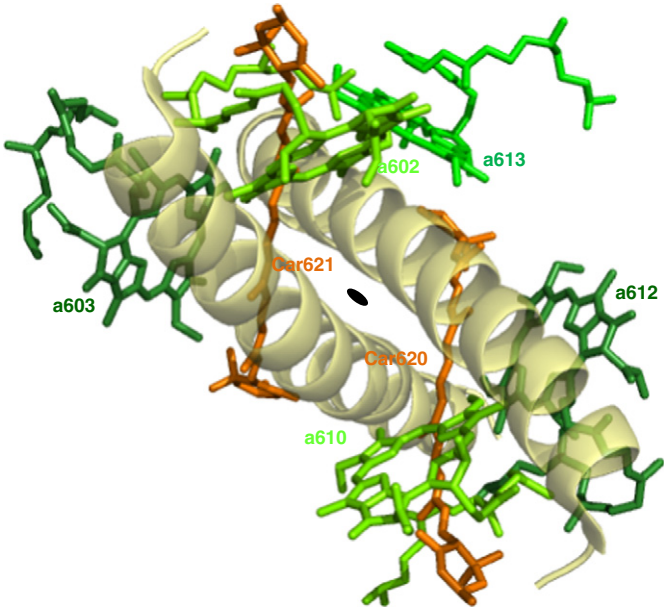

Fig. 9. Structural model of the pigments associated with the core basic unit of the LHC-II complex derived from PDB ID:1RWT. Only chlorophyll (green) and carotenoid (orange) binding sites conserved in VCP are shown. Car620 is located in site L1 and Car 621 in site L2. The two-fold symmetry axis is shown. The two conserved α-helices are shown in ribbons.

by LHC-II (a602, a603, a610, a612 and a613) are found conserved in all proteins. The six Chl *b* binding sites are in general not conserved, suggesting that this part of the protein was not maintained in different LHCs. This is consistent with the observed minor sequence homology of the C helix [43].

Due to the structural role played by luteins in sites L1 and L2 of LHC-II [46], these two sites, which are in proximity of the two conserved A and B helixes, are expected to be occupied by carotenoids also in VCP (Fig. 9). The most probable carotenoid for the occupancy of the L1 and L2 sites is violaxanthin, since vaucheriaxanthin has a bulky esterified chain, which cannot be accommodated in the core of the structure [17].

In LHC-II there are two other carotenoid binding sites: the N1 site which binds neoxanthin and the V1 site which binds violaxanthin. Both these carotenoids are located in the Chl *b* rich region of the LHC-II structure, and thus this part of the protein may differ substantially in VCP, which lacks this kind of pigment. Sequence analysis thus suggests that VCP shows a conserved nucleus of pigments, comprising carotenoids in L1, L2 sites and five Chl *a* molecules, as already suggested for FCP from *C. meneghiniana* [20] and LHC from the dinoflagellate *A. carterae* [21]. The conserved pigments of the core are shown in Fig. 9.

On the basis of this structural analogy, we suggest that the ^{3}Car contributions, observed in the ODMR, TR-EPR and FSE spectra, are due to the two carotenoids located in L1 and L2 sites, *i.e.* the same which are able to quench ^{3}Chl in LHC-II. To verify if this hypothesis is compatible with the experimental data, we have calculated the ^{3}Car EPR spectrum inherited through a TTET mechanism from the different Chls in the conserved protein core, and compared the results with TR-EPR and FSE experimental spectra, as reported in the next section.

3.5. TTET

The polarization pattern of the ^{3}Car is inherited from the ^{3}Chl donor during TTET in a way which is determined by the relative orientation of the acceptor–donor pair, therefore depending on the pigment arrangement inside the protein scaffold For both the carotenoids in L1 and L2 sites, the polarization pattern has been calculated considering all the nearby Chls (*i.e.* the conserved Chls at a distance closer than 4 Å), as possible triplet donors (namely Chl *a* 602–603–610–612–613). This calculation has been performed in the spin polarization conservation frame, with a program developed by the research group and previously used to interpret the TTET process relatively to other antenna systems [20–22]. The ZFS parameters of the ^{3}Car used for the TR-EPR spectra are slightly different from the parameters determined by ODMR but this dissimilarity may be ascribable to the different temperature at which the two kinds of measurements have been carried out.

From the comparison of the calculated spectra with the experimental FSE spectrum (the ^{3}Car component reported in Fig. 7) (Fig. 10), it can be seen that the best agreement is reached by considering, in the TTET process, the couples Chl *a* 603/Car 621 and Chl *a* 612/Car 620 as in LHC-II [22]. Note that the calculated ^{3}Car spectrum is the same for Chl *a* 603 and Chl *a* 612 as triplet donors, because of the symmetry of the pigment arrangement. The same calculated ^{3}Car spectrum has also been used in the reconstruction of the TR-EPR together with the "unquenched" ^{3}Chl contribution (Fig. 11, Table 3), giving a good agreement between calculated and experimental spectra. Thus, the observed consistency between model and experimental data strongly support the

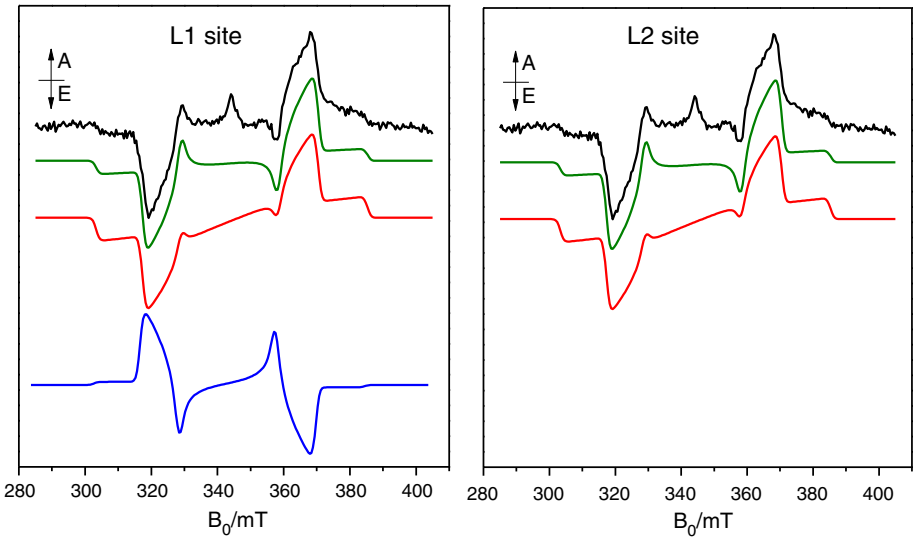

Fig. 10. Triplet spin-polarized spectra for violaxanthin in L1 (at left) and L2 (at right) calculated as populated by TTET from the triplet state of all the conserved Chl *a* in the protein core. The initial donor ^{3}Chl polarization is *eeeaaa* (P_x:P_y:P_z = 0.375:0.425:0.200). The spectra are compared to the carotenoid component of the experimental FSE spectrum reported in Fig. 7. Red line: Chl *a*602/Chl *a*610 right/left panels. Green line: Chl *a*603/Chl *a*612 right/left panels. Blue line: Chl *a*613.

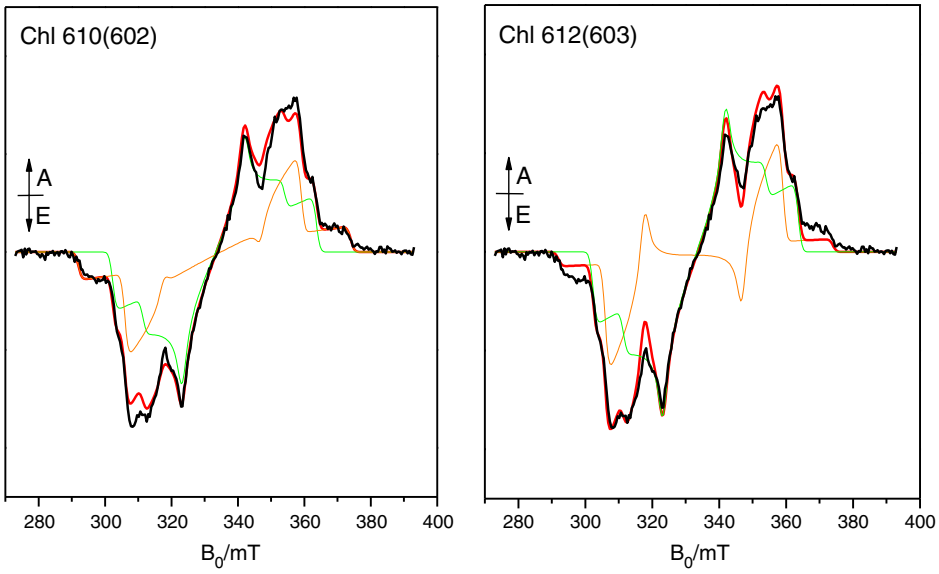

Fig. 11. Reconstruction (red) of the TR-EPR spectrum of monomeric VCP (black) as a sum of ^{3}Chl (green) and ^{3}Car (orange). The carotenoid contribution is the same as in Fig. 10, *i.e.* calculated according to TTET, starting from triplet states localized in Chl *a* 612 (left) and Chl *a* 610 (right). Parameters of the reconstruction are reported in Table 3.

idea that the pigments involved in ^{3}Chl quenching are indeed organized similarly in VCP and LHC-II.

4. Discussion

VCP was characterized, until now, only by steady state absorption and fluorescence [16,17,43]. Our approach, based on a combined investigation by ODMR and EPR spectroscopies, has allowed us to identify and characterize the different Chl and Car triplet states generated under photo-excitation. The results give detailed information on the photoprotection mechanism taking place in the light harvesting complex of the microalga *N. gaditana*, and may be compared to those available for other antenna complexes.

4.1. Photoprotective carotenoids

The two ^{3}Car contributions observed in the T−S and FDMR spectra of monomeric and trimeric VCP are assigned, as in the case of LHC-II, to the two core carotenoids located in L1 and L2 sites. In fact, the T−S spectra are very similar to those reported for LHC-II, [35,36,39] (Fig. S1, Supplementary material), suggesting also that sites L1 and L2 in VCP are most likely occupied by violaxanthin which has a molecular structure very similar to that of lutein. It has been suggested that, in the FCP complex, fucoxanthin molecules performing TTET are also located in analogous L1, L2 sites [19,20,47,48]. The difference in the optical properties of the two ^{3}Cars, observed in the ODMR spectra of VCP, is most likely due to the effect induced by the binding sites (L1 *vs* L2) rather than to different carotenoids. Two lutein triplet states having different optical properties, (T–T absorption at 510 nm (L1) and 530 nm (L2)), have been previously observed in LHC-II [35,39] and, similarly, two violaxanthin triplet states, showing different optical features (T–T absorption at 501 and 516 nm respectively), are detected in VCP.

Some differences in the ^{3}Car T−S spectrum of VCP with respect to the LHC-II one, are found in the Chl *a* absorption region. One is the absence of bands assigned in LHC-II to Chl *b*, as expected. The other difference is that the bleaching bands, attributed to two Chl *a* molecules interacting with the carotenoids located in sites L1and L2 respectively, are well resolved in LHC-II, while in VCP they are largely overlapping. This may be due to the absence of Chl *a* 611 in one site and of Chl *b* 609 on the other, which may slightly alter the electronic interactions among pigments and consequently their absorption frequency. Except for these differences, the analogy with LHC-II is strongly supported by the polarization pattern, in the TR-EPR and FSE spectra, of the ^{3}Car component which corresponds to that derived from TTET calculations for ^{3}Car formation in sites L1 and L2 starting from ^{3}Chl *a* 603/612.

4.2. Unquenched chlorophyll triplet states

As revealed by ODMR and EPR, a number of ^{3}Chls which are not transferring the triplet excitation to Cars are present, both in trimeric and monomeric VCP. Different triplet pools have been recognized, by fitting the ODMR data with three components and the addition of a minor fourth component for the monomeric VCP. The presence of this fourth red component is likely due to a lack of energy transfer among monomers, leading to an extra energy trap.

When compared to LHC-II, where unquenched ^{3}Chls have also been detected [30], VCP seems to be more exposed to this kind of ^{3}Chl generation, as suggested by the ODMR and EPR results. Blue and red Chls are both sites of triplet localization, as proven by the analysis of the T−S spectra. ^{3}Chls are a possible source of photoxidative damage. However some of the detected ^{3}Chl are likely not populated in physiological conditions, when the excitation is funneled to the reaction centers. It is worth noting that carotenoids are also able to quench directly the $^1O_2$ eventually produced *in situ* by ^{3}Chl, limiting in this way the possible damage to the apparatus *in vivo*. Moreover, in strong light conditions, when the probability to form ^{3}Chl states increases, due to the saturation of the reaction centers, additional mechanisms of photo-protection, as Non Photochemical quenching (NPQ), are also activated, to safely dissipate excess Chl singlet states, thus reducing ^{3}Chl formation and light induced damage [49]. Furthermore, in stressful conditions, when the photosynthetic apparatus is more prone to the accumulation of triplet states, *N. gaditana* shows a large PS I/PS II ratio, equal to 1.7 [50]. The predominance of PS I leads to the capability to set up a strong cyclic electron transfer and contributes to the dissipation of the excitation in excess, preserving the system. Thus, both the NPQ response and the enhanced cyclic electron transport may compensate the occurrence of ^{3}Chls observed in *N. gaditana* antennae.

At difference with LHC-II from higher plants, where the trimerization produces a strong effect in the optical properties, in VCP oligomerization does not substantially affect the FDMR and T−S spectra. A similar result has been obtained by absorption spectroscopy [17]. Our

experimental data thus support the hypothesis that in native VCP the interaction among monomers does not involve interfacial pigments.

5. Conclusions

The detailed analysis of the ODMR and EPR triplet spectra in VCP has revealed that, as in all the other homologous light harvesting complexes belonging to the LHC superfamily, carotenoids in L1 and L2 sites are devoted to ^{3}Chl quenching. These two central carotenoids, surrounded by five Chlorophyll *a* molecules, are found conserved in several other light harvesting complexes, which also show similar ^{3}Car quenching capability. This suggests that, although these antenna proteins have differentiated sequences and bind different pigments, in all members of the LHC superfamily there is a protein core with a conserved structural organization with a fundamental relevance for the photoprotective function.

We have also shown that red Chls are present in VCP, suggesting either the presence of interactions between Chls, although a significant packing of pigments seems to be unlikely due to the absence of Chl *b* and a limited number of Chl *a* molecules, or more likely to pronounced site energy effects. Trimerization of the protein does not lead to a significant effect either on the interaction among peripheral pigments or on the rearrangement of the chromophores inside the complexes.

Acknowledgements

We thank Dr. Lorenzo Franco for performing the TR-EPR experiments. This work was supported by the Italian Ministry for University and Research (MURST) under the project PRIN2010-2011 (2010FM738P_004). TM acknowledges ERC starting grant BIOLEAP nr 309485.

Appendix A. Supplementary data

Supplementary data to this article can be found online at http://dx.doi.org/10.1016/j.bbabio.2014.03.014.

References

[1] S. Sadekar, J. Raymond, R.E. Blankenship, Conservation of distantly related membrane proteins: photosynthetic reaction centers share a common structural core, Mol. Biol. Evol. 23 (2006) 2001–2007.
[2] J. Engelken, H. Brinkmann, I. Adamska, Taxonomic distribution and origins of the extended LHC (light-harvesting complex) antenna protein superfamily, BMC Evol. Biol. 10 (2010) 233.
[3] A.G. Koziol, T. Borza, K.I. Ishida, P. Keeling, R.W. Lee, D.G. Durnford, Tracing the evolution of the light-harvesting antennae in chlorophyll a/b-containing organisms, Plant Physiol. 143 (2007) 1802–1816.
[4] J.A. Neilson, D.G. Durnford, Structural and functional diversification of the light-harvesting complexes in photosynthetic eukaryotes, Photosynth. Res. 106 (2010) 57–71.
[5] Z. Liu, H. Yan, K. Wang, T. Kuang, J. Zhang, L. Gui, X. An, W. Chang, Crystal structure of spinach major light-harvesting complex at 2.72 Å resolution, Nature 428 (2004) 287–292.
[6] A. Busch, M. Hippler, The structure and function of eukaryotic photosystem I, Biochim. Biophys. Acta Bioenerg. 1807 (2011) 864–877.
[7] S.M. Dittami, G. Michel, J. Collen, C. Boyen, T. Tonon, Chlorophyll-binding proteins revisited—a multigenic family of light-harvesting and stress proteins from a brown algal perspective, BMC Evol. Biol. 10 (2010) 365.
[8] T. Veith, J. Brauns, W. Weisheit, M. Mittag, C. Büchel, Identification of a specific fucoxanthin–chlorophyll protein in the light harvesting complex of photosystem I in the diatom Cyclotella meneghiniana, Biochim. Biophys. Acta Bioenerg. 1787 (2009) 905–912.
[9] J.M. Archibald, P.J. Keeling, Recycled plastids: a 'green movement' in eukaryotic evolution, Trends Genet. 18 (2002) 577–584.
[10] L. Rodolfi, Z.G. Chini, N. Bassi, G. Padovani, N. Biondi, G. Bonini, M.R. Tredici, Microalgae for oil: strain selection, induction of lipid synthesis and outdoor mass cultivation in a low-cost photobioreactor, Biotechnol. Bioeng. 102 (2009) 100–112.
[11] R. Radakovits, R.E. Jinkerson, S.I. Fuerstenberg, H. Tae, R.E. Settlage, J.L. Boore, M.C. Posewitz, Draft genome sequence and genetic transformation of the oleaginous alga *Nannochloropsis gaditana*, Nat. Commun. 3 (2012) 686–695.
[12] E. Sforza, D. Simionato, G.M. Giacometti, A. Bertucco, T. Morosinotto, Adjusted light and dark cycles can optimize photosynthetic efficiency in algae growing in photobioreactors, PLoS ONE 7 (2012) e38975.
[13] G. Britton, S. Liaaen-Jensen, H. Pfander, Carotenoids Handbook, Birkhäuser Verlag, Basel, Switzerland, 2004.
[14] A. Hager, H. Stransky, Das Carotinoidmuster und die Verbreitung des lichtinduzierten Xanthophyllcyclus in verschiedenen Algenklassen. III. Grunalgen. Arch. Microbiol. 72 (1970) 68–83.
[15] O. Mangoni, C. Imperatore, C.R. Tomas, V. Costantino, V. Saggiomo, A. Mangoni, The new carotenoid pigment moraxanthin is associated with toxic microalgae, Mar. Drugs 9 (2011) 242–255.
[16] A. Sukenik, A. Livne, A. Neori, Y.Z. Yacobi, D. Katcoff, Purification and characterization of A light-harvesting chlorophyll–protein complex from the marine eustigmatophyte Nannochloropsis sp, Plant Cell Physiol. 33 (1992) 1041–1048.
[17] S. Basso, D. Simionato, C. Gerotto, A. Segalla, G.M. Giacometti, T. Morosinotto, Characterization of the photosynthetic apparatus of the Eustigmatophycean *Nannochloropsis gaditana*: evidence of convergent evolution in the supramolecular organization of photosystem I, Biochim. Biophys. Acta Bioenerg. 1837 (2014) 306–314.
[18] E.J. Land, A. Sykes, T.G. Truscott, The in vitro photochemistry of biological molecules —II. The triplet states of β-carotene and lycopene excited by pulse radiolysis, Photochem. Photobiol. 13 (1971) 311–320.
[19] M. Di Valentin, C. Büchel, G.M. Giacometti, D. Carbonera, Chlorophyll triplet quenching by fucoxanthin in the fucoxanthin–chlorophyll protein from the diatom *Cyclotella meneghiniana*, Biochem. Biophys. Res. Commun. 427 (2012) 637–641.
[20] M. Di Valentin, E. Meneghin, L. Orian, A. Polimeno, C. Büchel, E. Salvadori, W.M.K. Kay, D. Carbonera, Triplet–triplet energy transfer in fucoxanthin–chlorophyll protein from diatom *Cyclotella meneghiniana*: insights into the structure of the complex, Biochim. Biophys. Acta Bioenerg. 1827 (2013) 1226–1234.
[21] M. Di Valentin, E. Salvadori, G. Agostini, F. Biasibetti, S. Ceola, R. Hiller, G.M. Giacometti, D. Carbonera, Triplet–triplet energy transfer in the major intrinsic light-harvesting complex of *Amphidinium carterae* as revealed by ODMR and EPR spectroscopies, Biochim. Biophys. Acta Bioenerg. 1797 (2010) 1795-1767.
[22] M. Di Valentin, F. Biasibetti, S. Ceola, D. Carbonera, Identification of the sites of chlorophyll triplet quenching in relation to the structure of LHC-II from higher plants. Evidence from EPR Spectroscopy, J. Phys. Chem. B 113 (2009) 13071–13078.
[23] M. Di Valentin, S. Ceola, G. Agostini, G.M. Giacometti, A. Angerhofer, O. Crescenzi, V. Barone, D. Carbonera, Pulse ENDOR and density functional theory on the peridinin triplet stateinvolved in the photo-protective mechanism in the peridinin–chlorophyll a–protein from *Amphidinium carterae*, Biochim. Biophys. Acta Bioenerg. 1777 (2008) 295–307.
[24] M. Di Valentin, C. Tait, E. Salvadori, S. Ceola, H. Scheer, R.G. Hiller, D. Carbonera, Conservation of spin polarization during triplet–triplet energy transfer in reconstituted peridinin–chlorophyll–protein complexes, J. Phys. Chem. B 115 (2011) 13371–13380.
[25] R.R.L. Guillard, J.H. Ryther, Studies of marine planktonic diatoms. I. Cyclotella nana Hustedt and Detonula confervagea Cleve, Can. J. Microbiol. 8 (1962) 229–239.
[26] P. Di Tommaso, S. Moretti, I. Xenarios, M. Orobitg, A. Montanyola, J.M. Chang, J.F. Taly, J.F.C. Notredame, T-Coffee: a web server for the multiple sequence alignment of protein and RNA sequences using structural information and homology extension, Nucleic Acids Res. 39 (2011) W13–W17.
[27] C. Notredame, D.G. Higgins, J. Heringa, T-Coffee: A novel method for fast and accurate multiple sequence alignment, J. Mol. Biol. 302 (2000) 205–217.
[28] C.E. Corteggiani, A. Telatin, N. Vitulo, C. Forcato, M. D'Angelo, R. Schiavon, A. Vezzi, G. M. Giacometti, T. Morosinotto, G. Valle, Chromosome scale genome assembly and trascriptome profiling of *Nannochloropsis gaditana* in nitrogen depletion, Mol. Plant (2014) 323–335.
[29] D. Carbonera, Optically detected magnetic resonance (ODMR) of photoexcited triplet states, Photosynth. Res. 102 (2009) 403–414.
[30] D. Carbonera, G. Giacometti, G. Agostini, FDMR of carotenoid and chlorophyll triplets in light harvesting complex LHC II of spinach, Appl. Magn. Reson. 3 (1992) 859–872.
[31] S. Santabarbara, E. Bordignon, R.C. Jennings, D. Carbonera, Chlorophyll triplet states associated with photosystem II of thylakoids, Biochemistry 41 (2002) 8184–8194.
[32] H.C. Brenner, J.C. Brock, C.B. Harris, Energy exchange in a coherently coupled ensemble, Chem. Phys. 31 (1978) 137–164.
[33] S. Stoll, A. Schweiger, EasySpin, a comprehensive software package for spectral simulation and analysis in EPR, J. Magn. Reson. 178 (2006) 42–55.
[34] D. Carbonera, G. Giacometti, G. Agostini, FDMR spectroscopy of peridinin–chlorophyll-a protein from *Amphidinium carterae*, Spectrochim. Acta 51A (1995) 115–123.
[35] R. van der Vos, D. Carbonera, A.J. Hoff, Microwave and optical spectroscopy of carotenoid triplets in light-harvesting complex LHC-II of spinach by absorbance-detected magnetic resonance, Appl. Magn. Reson. 2 (1991) 179–202.
[36] S.S. Lampoura, V. Barzda, G.M. Owen, A.J. Hoff, H. van Amerongen, Aggregation of LHCII leads to a redistribution of the triplets over the central xanthophylls in LHCII, Biochemistry 4 (2002) 9139–9144.
[37] A. Angerhofer, F. Bornhäuser, A. Gall, R.J. Cogdell, Optical and optically detected magnetic resonance investigation on purple photosynthetic bacterial antenna complexes, Chem. Phys. 194 (1995) 259–274.
[38] D. Carbonera, G. Giacometti, G. Agostini, A. Angerhofer, V. Aust, ODMR of carotenoid and chlorophyll triplets in CP43 and CP47 complexes of spinach, Chem. Phys. Lett. 194 (1992) 275–281.
[39] D. Carbonera, G. Giacometti, Optically detected magnetic resonance of pigments in light harvesting complex (LHCII) of spinach, Ren. Fis. Acc. Lincei 3 (1992) 361–368.
[40] O. Gonen, H. Levanon, Line–shape analysis of transient triplet electron paramagnetic resonance spectra. Application to porphyrins and chlorophylls in nematic uniaxial liquid crystals, J. Phys. Chem. 88 (1984) 4223–4228.
[41] D. Carbonera, M. Di Valentin, G. Agostini, G. Giacometti, P.A. Liddel, D. Gust, A.L. Moore, T.A. Moore, Energy transfer and spin polarization of the carotenoid triplet state in synthetic carotenoporphyrin dyads and in natural complexes, Appl. Magn. Reson. 13 (1997) 487–504.
[42] R. Bittl, E. Schlodder, I. Geisenheimer, W. Lubitz, R.J. Cogdell, Transient EPR and absorption studies of carotenoid triplet formation in purple bacterial antenna complexes, J. Phys. Chem. B 105 (2001) 5525–5535.

[43] A. Sukenik, A. Livne, K.E. Apt, A.R. Grossman, Characterization of a gene encoding the light-harvesting violaxanthin–chlorophyll protein of *Nannochloropsis* sp. (*Eustigmatophyceae*), J. Phycol. 36 (2000) 563–570.
[44] D.G. Durnford, J.A. Deane, S. Tan, G.I. McFadden, E. Gantt, B.R. Green, A phylogenetic assessment of the eukaryotic light-harvesting antenna proteins, with implications for plastid evolution, J. Mol. Evol. 48 (1999) 59–68.
[45] T. Cavalier-Smith, Only six kingdoms of life, Proc. R. Soc. Lond. B 271 (2004) 1251–1262.
[46] H. Paulsen, U. Rümler, W. Rüdiger, Reconstitution of pigment-containing complexes from light-harvesting chlorophyll a/b-binding protein overexpressed in *Escherichia coli*, Planta 181 (1990) 204–211.
[47] L. Premvardhan, L. Bordes, A. Beer, C. Büchel, B. Robert, Carotenoid structures and environments in trimeric and oligomeric fucoxanthin chlorophyll a/c2 proteins from resonance Raman spectroscopy, J. Phys. Chem. B 113 (2009) 12565–12574.
[48] L. Premvardhan, B. Robert, A. Beer, C. Büchel, Pigment organization in fucoxanthin chlorophyll a/c(2) proteins (FCP) based on resonance Raman spectroscopy and sequence analysis, Biochim. Biophys. Acta Bioenerg. 1797 (2010) 1647–1656.
[49] S. Cao, X. Zhang, D. Xu, X. Fan, S. Mou, Y. Wang, N. Ye, W. Wang, A transthylakoid proton gradient and inhibitors induce a non-photochemical fluorescence quenching in unicellular algae *Nannochloropsis* sp, FEBS Lett. 587 (2013) 1310–1315.
[50] D. Simionato, S. Basso, G.M. Giacometti, T. Morosinotto, Optimization of light use efficiency for biofuel production in algae, Biophys. Chem. 182 (2013) 71–78.